

REAL: Representation Enhanced Analytic Learning for Exemplar-Free Class-Incremental Learning

Run He ^a, Di Fang ^b, Yizhu Chen ^b, Kai Tong ^a, Cen Chen ^b, Yi Wang ^c, Lap-pui Chau ^c, Huiping Zhuang ^{a,*}

^aShien-Ming Wu School of Intelligent Engineering, South China University of Technology, GuangZhou, China

^bSchool of Future Technology, South China University of Technology, GuangZhou, China

^cDepartment of Electrical and Electronic Engineering, The Hong Kong Polytechnic University, Hong Kong SAR, China

Abstract

Exemplar-free class-incremental learning (EFCIL) aims to mitigate catastrophic forgetting in class-incremental learning (CIL) without relying on historical training samples as exemplars. Compared with exemplar-based CIL that stores exemplars, EFCIL is more prone to forgetting. An emergent EFCIL branch named Analytic Continual Learning (ACL) introduces a gradient-free paradigm based on Recursive Least-Square for forgetting-resistant classifier training with a frozen backbone during CIL. However, ACL currently suffers from ineffective representations and limited utilization of backbone knowledge. To address these challenges, we propose a representation-enhanced analytic learning (REAL) scheme. REAL improves the representation by constructing a dual-stream base pretraining stage followed by a representation-enhancing distillation process. The dual-stream base pretraining combines self-supervised contrastive learning for general features with supervised learning for class-specific knowledge, followed by representation-enhancing distillation to integrate both streams, improving representations for the subsequent CIL paradigm. REAL further introduces a feature fusion buffer to multi-layer backbone features, enabling richer feature extraction for classifier training. Our proposed method can be incorporated into existing ACL techniques, yielding superior performance. Empirical results demonstrate that REAL achieves state-of-the-art performance on CIFAR-100, ImageNet-100, and ImageNet-1k benchmarks, outperforming existing exemplar-free methods and rivaling exemplar-based approaches.

Keywords:

Class-Incremental Learning, Exemplar-Free, Analytic Learning, Representation Enhancement, Feature Fusion.

1. Introduction

Continual learning [1, 2, 3], also known as incremental learning, enables models to acquire knowledge from sequentially arriving data in a phase-by-phase manner. This process resembles the human learning, where new information is continuously assimilated into existing knowledge. Similarly, continual learning is crucial for the accumulation of machine intelligence in real-world scenarios. Class-incremental learning (CIL) [4, 5], a typical scenario of continual learning, has gained increasing popularity owing to its ability to continuously adapt trained networks to previously unseen classes. The approach recognizes that certain data categories may be limited to certain locations or time slots, thereby enabling models to learn without resource-intensive joint retraining.

Despite these advantages, CIL suffers from *catastrophic forgetting* [6], where models rapidly lose previously learned knowledge when acquiring new information. Various solutions have been proposed to alleviate this issue. Among them, exemplar-based CIL (EBCIL) has demonstrated competitive results by storing historical samples as exemplars to help retain old knowledge while learning new data. However, this strategy

introduces notable privacy concerns. By contrast, exemplar-free CIL (EFCIL) avoids storing previous samples, thus eliminating the privacy issue; however, it experiences more severe forgetting. The difference between EBCIL and EFCIL is illustrated in Figure 1.

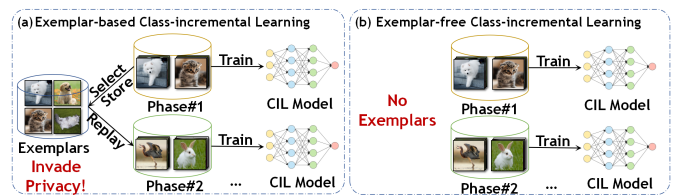


Figure 1: The difference between EBCIL and EFCIL. At each phase, EBCIL utilizes the stored exemplars selected from previous categories to train the model (as shown in (a)), while EFCIL does not keep exemplars and uses the categories within the training phase (i.e., in (b)).

Recently, a new branch of EFCIL termed analytic continual learning (ACL) [7] has effectively addressed the catastrophic forgetting and has shown promising results while adhering to the exemplar-free constraint. ACL introduces a framework where a backbone is first trained using back-propagation (BP) in the base phase. Subsequently, a linear classifier is trained incrementally phase by phase with a recursive paradigm. The recursive paradigm leverages analytic learning (AL) [8, 9, 10]

*Corresponding author: hpzhuang@scut.edu.cn

to train neural networks with closed-form solutions and offers a *weight-invariant property*. This property indicates that weights trained recursively in each phase are identical to those trained simultaneously on the entire data [7, 11]. ACIL incorporates this property into the CIL to achieve highly competitive results, particularly in large-phase scenarios (e.g., 50 phases) [7]. The weight-invariant property also maintains almost the same results across different scenarios of phases. Moreover, a fixed memory footprint for storing previous information in ACL enables ACL to operate in extreme scenarios (e.g., learning one category in a phase [12]).

However, existing ACL techniques have two limitations: (1) The feature representations are less effective on unseen categories after the base phase, which limits performance in future phases. Existing ACL methods employ supervised learning to acquire representation and freeze the backbone after the base phase, resulting in less discriminative representations across unseen data categories. (2) The classifier does not effectively utilize the knowledge captured by the backbone. Existing ACL trains the classifier with the final output of the backbone. Features extracted by different layers of backbones can contain varying semantic information. For convolutional neural networks (CNNs) that are widely used in CIL tasks, deep features are generally more specific to the current task (i.e., classes in the current learning phase for CIL), whereas shallow features tend to be more transferable [13]. Learning solely with the final output may overlook potential improvements that can be achieved with transferable shallow features. These limitations highlight the importance of exploring potential approaches to enhance representation learning and feature utilization of ACL. For representation enhancement, general knowledge learned without labels can benefit incremental learning [14]. Additionally, self-supervised contrastive learning (SSCL) [15] has shown effectiveness in learning general representations. SSCL learns general representations through contrastive proxy tasks, and these learned representations can be effectively adapted to downstream tasks. As the model is initially trained in a base phase and then incrementally learns new tasks, general representations have the potential to enhance the ACL process. In terms of knowledge utilization, leveraging knowledge with different semantic information, particularly transferable features, can enhance classifier training in ACL.

Herein, we propose **Representation Enhanced Analytic Learning (REAL)** for EFCIL to enhance the representation and knowledge utilization of ACL. Based on the shared objectives of SSCL and CIL, REAL aims to improve the representation of the backbone for unseen categories by integrating label-guided knowledge and general knowledge. Structurally, a dual-stream base pretraining (DS-BPT) is conducted for backbones during the base phase to capture general knowledge via SSCL and learn supervised feature distribution via SL. Following DS-BPT, a representation-enhancing distillation (RED) process is employed to collaboratively merge both types of knowledge to further enhance the model. Consequently, a more robust backbone with improved representations is established for subsequent ACL. Moreover, REAL enhances the utilization of backbone knowledge by introducing a feature fusion buffer (FFB)

to leverage features extracted from different layers of the CNN backbone. The FFB employs a feature fusion process to construct informative feature vectors that facilitate classifier training. REAL advances the ACL family by enhancing representation extraction without compromising fundamental benefits, such as the weight-invariant property. These proposed techniques are designed to seamlessly integrate into existing ACL frameworks. The key contributions of REAL are summarized as follows,

- We introduce DS-BPT and RED to address the representation limitation in ACL. DS-BPT pretrains backbones in two streams using both SL and SSCL to acquire knowledge from both general and specific information. RED merges knowledge obtained from DS-BPT, constructing a backbone that encapsulates both types of knowledge, enabling the backbone to further refine its representation while retaining general knowledge.
- We propose FFB to overcome the challenge of knowledge utilization by constructing more informative features. FFB introduces mid-layer information by compressing information of different channels to a layer-wise feature map. Subsequently, the compressed feature maps extracted from different layers of the backbone are fused to create feature vectors, combining transferable and specific features for classifier learning.
- The components introduced in REAL can be seamlessly integrated into existing ACL methods, which makes REAL a versatile technique to enhance existing ACL approaches.
- Experimental results on various benchmark datasets demonstrate that REAL achieves remarkable performance, outperforming state-of-the-art EFCIL methods and several EBCIL methods.

The remaining contents of this paper are organized as follows. Section 2 reviews the related works. Our method, namely REAL, is depicted in Section 3. In Section 4, experiments are conducted to validate and analyze the performance of REAL. Section 5 concludes this paper.

2. Related Works

In this section, we provide a comprehensive review of CIL techniques covering both EBCIL and EFCIL methods. Additionally, SSCL, which is closely related to the proposed REAL, is also discussed.

2.1. Exemplar-Based CIL

EBCIL, first introduced by iCaRL [5], reinforces models' memory by replaying historical exemplars via a herding mechanism for selecting exemplars. The exemplars are a fraction of encountered data stored in a fixed memory. Such a replay mechanism has gained popularity with various subsequent attempts [16, 17]. Various studies have leveraged knowledge distillation

(KD) to gain better replay. For instance, LUCIR [18] adjusts the feature to a sphere surface with cosine similarity and uses KD to maintain the orientations of features. PODNet [19] implements an efficient spatial-based distillation loss to reduce forgetting. FOSTER [20] employs a two-stage learning paradigm with KD, expanding and then reducing the network to the original size. In addition, numerous studies have investigated the management of memory. MIR [21] constructs a better exemplar set within limited memory by selecting samples that have a large impact on loss. GDumb [22] greedily stores samples while keeping the classes balanced. RMM [23] leverages reinforcement learning to dynamically manage memory for exemplars. The scope of stability-plasticity balance during replaying was also studied. AANets [24] integrates a stable block and a plastic block to balance stability and plasticity. Additionally, online hyperparameter optimization [25] adaptively optimizes the stability-plasticity balance without prior knowledge. Although the EBCIL provides generally good results, it invades privacy and requires additional memory to store exemplars.

2.2. Exemplar-Free CIL

Compared with EBCIL, EFCIL addresses catastrophic forgetting without the using exemplars to alleviate the privacy problem. It can be categorized into regularization-based CIL [26, 27, 28], prototype-based CIL [29, 30, 31], and the recently proposed ACL [7, 12, 11].

Regularization-based CIL imposes additional constraints on network activations or key parameters to mitigate forgetting. KD is introduced as a typical method to construct the constraint between old and new models. For example, LwF [4] prevents activation changes between old and new networks via KD, and LwM [32] introduces an attention distillation loss. Other approaches set constraints related to important weights of previous tasks, and several researches have studied how to model the importance. For example, EWC [33] captures prior importance using a diagonally approximated Fisher information matrix. Building upon EWC, online EWC [28] reduces the accumulations of Fisher matrices in EWC. SI [34] calculates the impact of parameter change on loss via the path integral to determine important parameters. RWalk [35] combines the Fisher matrix in EWC and path integral in SI to compute the importance. Regularization-based CIL respects privacy without storing exemplars, but the constraint imposed on network updates prevents the model from learning new tasks.

Prototype-based CIL mitigates forgetting by storing prototypes to maintain decision boundaries across old and new tasks. The prototypes, typically the feature means of specific classes, are incorporated into classifier training to supply previous information. Multiple studies have investigated how to simulate past feature distributions from prototypes. For instance, PASS [36] augments the prototypes by adding Gaussian noise to balance between old and new categories. SSRE [37] introduces a prototype selection mechanism with up-sampling of prototypes to reduce feature confusion. FeTriL [38] introduces a mechanism to generate pseudo-features of old classes by estimating the difference of feature distributions from prototypes. However, these methods do not consider the fact that, old prototypes may be

inaccurate due to the evolution of models during incremental learning. PRAKA [14] addresses this problem by providing a prototype reminiscence mechanism that estimates the change of old prototypes. Moreover, NAPA-VQ [39] utilizes the neighborhood information in feature space to hold more compact decision boundaries between classes. As a prevalent branch recently proposed, the prototype-based CIL gains prominence in the EFCIL realm and achieves state-of-the-art performance. However, it favors stability with limited plasticity, and the storing of prototypes can be a large extra cost for large-class tasks.

ACL is a recently developed branch of EFCIL that aims to find closed-form solutions for all seen data. AL [8, 9, 10] utilizes least squares (LS) to yield closed-form solutions during the training of neural networks. ACIL [7] first introduces AL to the CIL realm. It is developed by reformulating the CIL procedure into a recursive LS form thereby equating the CIL with joint training in the linear classifier. The subsequent GKEAL [11] specializes in few-shot CIL settings by adopting a Gaussian kernel process that excels in data-scarce scenarios. DS-AL [12] introduces a compensation stream to address the fitting problem of the linear classifier in ACIL. The ACL family can tackle various scenarios, including online CIL [40], imbalanced CIL [41, 42], generalized CIL [43], and multi-modal tasks [44, 45]. While ACL demonstrates substantial performance, it relies on the performance of the backbone, which is trained solely on the base dataset in a supervised manner. This approach may result in inadequate representations of unseen data without future label guidance. Moreover, training solely with final features of the backbone diminishes the utilization of backbone knowledge, potentially impacting of ACL. This study introduces REAL to enhance ACL and mitigate these limitations.

2.3. Self-Supervised Contrastive Learning

SSCL [15] enables label-free learning via a contrastive manner. It encourages features of similar samples to get close and forces dissimilar ones to be apart. Generally, Siamese networks are constructed for contrastive learning. For instance, SimCLR [46] utilizes a symmetric Siamese network for contrastive training and MOCO [47] mitigates the influence of extreme samples through momentum updates. However, they require negative samples (samples in different classes) and large a batch size to train a good model. By contrast, BYOL [48] uses only positive samples by introducing auxiliary structures trained with momentum. Built upon BYOL, SimSiam [49] replaces the momentum mechanism with gradient stopping and achieves considerable performance with a small batch size. The models trained via SSCL learn to extract general representations and can be effectively transferred [50]. We utilize this technique to obtain the general base representations. Several studies has used contrastive learning to improve the performance of CIL [51, 52, 53]. However, these approaches either restrict the use of contrastive learning to EBCIL [51, 52], or rely solely on the knowledge acquired through SSCL during the incremental phases [53]. By contrast, REAL is the first method to integrate knowledge obtained from both SSCL and SL to enhance incremental learning within the EFCIL framework.

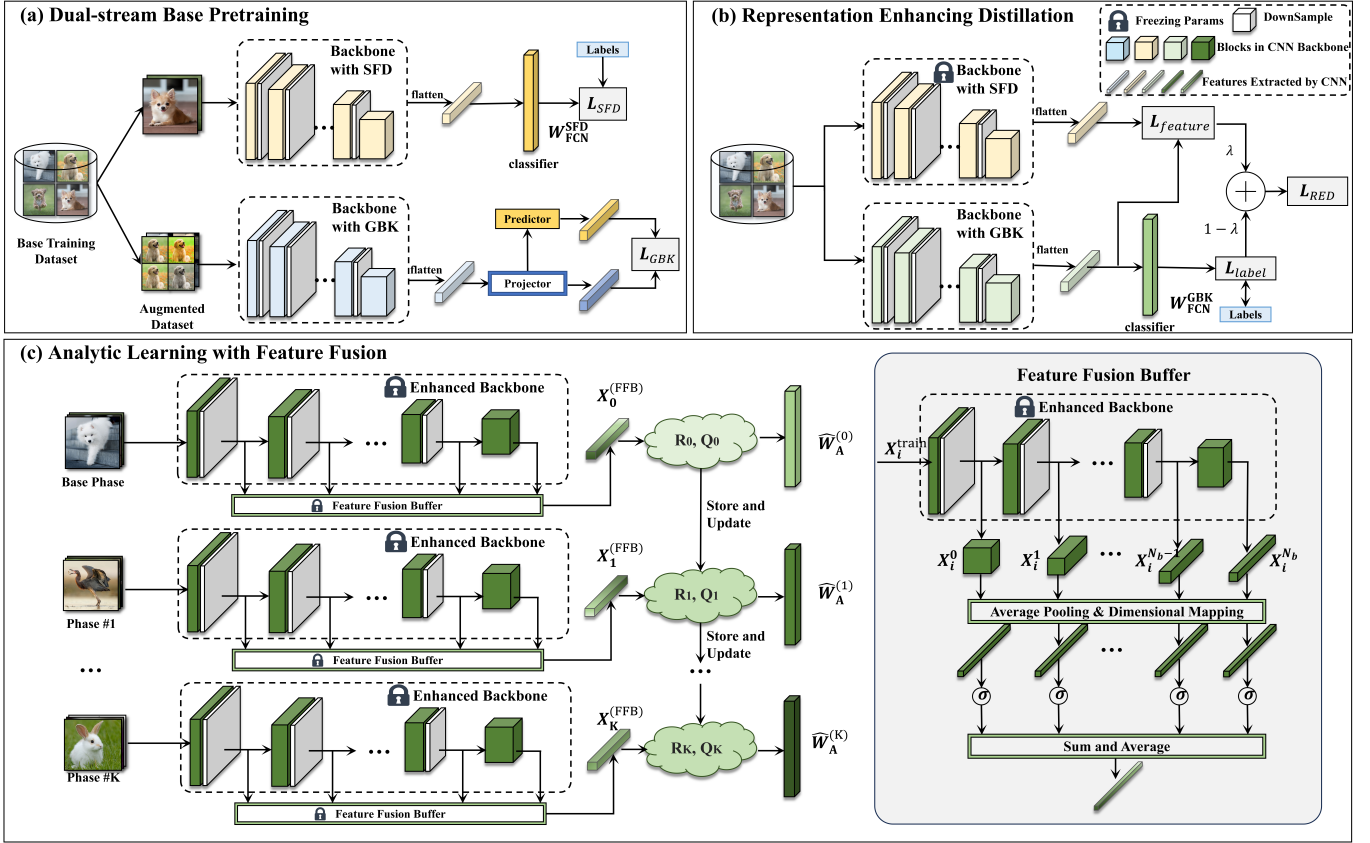


Figure 2: REAL focuses on enhancing the representation and backbone knowledge utilization during training and comprises three parts: (a) Dual-stream base pretraining (DS-BPT), (b) representation enhancing distillation (RED), and (c) analytic learning with feature fusion. Base knowledge is obtained by pretraining the CNN backbones with two streams. One stream acquires general base knowledge (GBK) via self-supervised contrastive learning (SSCL). The other learns supervised feature distribution (SFD) via supervised learning (i.e., in (a)). During RED, the backbone with SFD is frozen and transfers knowledge to the model with GBK via knowledge distillation (i.e., in (b)). Following base training, the enhanced backbone (i.e., backbone with GBK after RED) is embedded in the analytic learning agenda with a feature fusion buffer (i.e., in (c)).

3. Proposed Method

This section presents the details of the proposed REAL framework. The paradigm comprises three parts: Dual-stream Base Pretraining (DS-BPT), Representation Enhancing Distillation (RED) and Analytic Learning with Feature fusion (ALFF). An overview of REAL is depicted in Figure 2.3.

3.1. Dual-Stream Base Pretraining

Prior to further description, some definitions related to the CIL are presented. For CIL, the training data are given in a phase-by-phase manner with disjoint data categories. Suppose the CIL paradigm contains $K + 1$ phases, at each phase (e.g., phase k , $k = 0, \dots, K$), training data of disjoint classes $\mathcal{D}_k = \{\mathcal{X}_{k,i}, y_{k,i}\}_{i=1}^{N_k}$, where $\mathcal{X}_{k,i} \in \mathbb{R}^{c \times w \times h}$ represents the i -th input image in task k , $y_{k,i}$ denotes the label of the i -th input data, and N_k indicates the total number of samples in task t . In particular, $\mathcal{D}_0^{\text{train}} = \{\mathcal{X}_{0,i}^{\text{train}}, y_{0,i}^{\text{train}}\}_{i=1}^{N_0}$ represents the base training set and $\mathcal{D}_{0:k}$ represents the joint dataset from phase 0 to phase k . The objective of CIL at phase k is to train the model given $\mathcal{D}_k^{\text{train}}$ and test it on $\mathcal{D}_{0:k}^{\text{test}}$.

ACL suffers from less effective representation after the base phase. We propose dual-stream base pretraining at the base

phase to capture the both general base knowledge and specific supervised feature distribution (label-guided knowledge). Technically, the network is pretrained in streams of supervised learning and SSCL to obtain the base knowledge during base phase before a subsequent enhancement. Here we use a CNN as the backbone.

General Base Knowledge Acquisition. The GBK acquisition stream trains a backbone with GBK via the SSCL which decouples training from labels. We adopt SimSiam [49] as the SSCL architecture, which comprises a Siamese network of CNN backbone and formulates contrastive proxy tasks between different views (i.e., different augmentations of the same image).

Auxiliary structures, namely projector and predictor, are incorporated to assist SSCL training as extra mappings. The projector and predictor are multi-layer perceptrons (MLPs) that provide a diversified feature mapping benefiting the SSCL process. Suppose the stacked N_k -sample input tensor at phase 0 is X_0^{train} , and the random data augmentation operation is denoted as f_{RA} , two views of the input image tensors after data augmentation can be represented as $X^{\text{aug}_1} = f_{\text{RA}}(X_0^{\text{train}})$ and $X^{\text{aug}_2} = f_{\text{RA}}(X_0^{\text{train}})$. Let W_{proj} , W_{pred} , and $W_{\text{CNN}}^{\text{GBK}}$ represent the

weights of the projector, predictor, and the CNN backbone for GBK acquisition respectively. Given two views ($\mathbf{X}^{\text{aug}_1}$, $\mathbf{X}^{\text{aug}_2}$) of input $\mathbf{X} \in \mathbb{R}^{c \times w \times h}$, the outputs are,

$$\mathbf{X}^{\text{proj}_1} = f_{\text{proj}}(f_{\text{flat}}(f_{\text{CNN}}(\mathbf{X}^{\text{aug}_1}, \mathbf{W}_{\text{CNN}}^{\text{GBK}}) \mathbf{W}_{\text{proj}})), \quad (1)$$

$$\mathbf{X}^{\text{proj}_2} = f_{\text{proj}}(f_{\text{flat}}(f_{\text{CNN}}(\mathbf{X}^{\text{aug}_2}, \mathbf{W}_{\text{CNN}}^{\text{GBK}}) \mathbf{W}_{\text{proj}})), \quad (2)$$

$$\mathbf{X}^{\text{pred}_1} = f_{\text{pred}}(\mathbf{X}^{\text{proj}_1}, \mathbf{W}_{\text{pred}}), \quad (3)$$

$$\mathbf{X}^{\text{pred}_2} = f_{\text{pred}}(\mathbf{X}^{\text{proj}_2}, \mathbf{W}_{\text{pred}}), \quad (4)$$

where f_{CNN} indicates passing the image through the CNN backbone, f_{flat} represents a flattening operator, and f_{proj} and f_{pred} are operations of projector and predictor respectively.

We then optimize the negative cosine similarity of these features. For two tensors \mathbf{Z}_1 and $\mathbf{Z}_2 \in \mathbb{R}^{N \times d}$, the negative cosine similarity can be defined as

$$\mathcal{L}_{\text{cos}}(\mathbf{Z}_1, \mathbf{Z}_2) = - \sum_{i=1}^N \frac{\mathbf{z}_{1,i} \cdot \mathbf{z}_{2,i}}{\|\mathbf{z}_{1,i}\|_2 \|\mathbf{z}_{2,i}\|_2}, \quad (5)$$

where $\mathbf{z}_{j,i}$ represents a row vector of \mathbf{Z}_j ($i = 1, 2, \dots, N$; $j = 1, 2$), \cdot refers to the dot product operation, and $\|\cdot\|_2$ is the L2-norm. The loss function of GBK acquisition is

$$\mathcal{L}_{\text{GBK}} = \frac{1}{2} \mathcal{L}_{\text{cos}}(\mathbf{X}^{\text{proj}_1}, \mathbf{X}^{\text{pred}_2}) + \frac{1}{2} \mathcal{L}_{\text{cos}}(\mathbf{X}^{\text{proj}_2}, \mathbf{X}^{\text{pred}_1}), \quad (6)$$

and we can use BP to minimize \mathcal{L}_{GBK} to obtain a finely trained model.

Learning Supervised Feature Distribution. While we can capture the GBK via an SSCL process, the information derived from labels remains valuable. Supervised knowledge can serve as a beneficial complement, particularly when conducting CIL in a supervised manner. Here, we employ a learning stream to acquire specific knowledge, specifically focusing on supervised feature distribution through supervised learning. Suppose $\mathbf{W}_{\text{CNN}}^{\text{SFD}}$ and $\mathbf{W}_{\text{FCN}}^{\text{SFD}}$ represent the weights of the CNN backbone and fully-connected network (FCN), the output can be

$$\hat{\mathbf{Y}}^{\text{SFD}} = f_{\text{softmax}}(f_{\text{flat}}(f_{\text{CNN}}(\mathbf{X}_0^{\text{train}}, \mathbf{W}_{\text{CNN}}^{\text{SFD}})) \mathbf{W}_{\text{FCN}}^{\text{SFD}}). \quad (7)$$

With labels $\mathbf{Y}_0^{\text{train}}$, we can train the model via BP with the loss function of cross entropy. Following training, the backbone can generate the feature with certain distribution guided by labels. DS-BPT encodes both GBK and SFD into two backbones and then utilizes them in the subsequent procedures.

3.2. Representation Enhancing Distillation

Both general knowledge (GBK) and specific knowledge (SFD) are obtained after DS-BPT. Here, we introduce the RED process to leverage both types of knowledge to enhance the representation of the backbone.

We enhance the representation by transferring supervised knowledge through the extracted feature vectors using a KD process. The extracted feature vectors from two backbones can be obtained as

$$\mathbf{X}^{\text{GBK}} = f_{\text{flat}}(f_{\text{CNN}}(\mathbf{X}_0^{\text{train}}, \mathbf{W}_{\text{CNN}}^{\text{GBK}})), \quad (8)$$

$$\mathbf{X}^{\text{SFD}} = f_{\text{flat}}(f_{\text{CNN}}(\mathbf{X}_0^{\text{train}}, \mathbf{W}_{\text{CNN}}^{\text{SFD}})). \quad (9)$$

During the KD process, the backbone pretrained in the SFD is frozen to provide knowledge of feature distribution, while the backbone pretrained in the GBK stream assimilates the knowledge. This is accomplished by aligning the output features extracted by the GBK backbone with those extracted by the SFD model by minimizing the difference them. In particular, we utilize cosine similarity, i.e.,

$$\mathcal{L}_{\text{feature}} = - \frac{1}{N} \sum_{i=1}^N \frac{\mathbf{x}_i^{\text{SFD}} \cdot \mathbf{x}_i^{\text{GBK}}}{\|\mathbf{x}_i^{\text{SFD}}\|_2 \|\mathbf{x}_i^{\text{GBK}}\|_2}, \quad (10)$$

where $\mathbf{x}_i^{\text{SFD}}$ and $\mathbf{x}_i^{\text{GBK}}$ represent i -th row vectors of \mathbf{X}^{SFD} and \mathbf{X}^{GBK} respectively. The labels can serve as a valuable source of supervision for enhancing representations. We incorporate additional cross-entropy loss for classification to utilize the direct guidance offered by the labels. We introduce a linear classifier after the backbone to correlate the representations extracted by the backbones with the labels. The output of the model following this addition is denoted as

$$\hat{\mathbf{Y}}^{\text{GBK}} = f_{\text{softmax}}(f_{\text{flat}}(f_{\text{CNN}}(\mathbf{X}_0^{\text{train}}, \mathbf{W}_{\text{CNN}}^{\text{GBK}})) \mathbf{W}_{\text{FCN}}^{\text{GBK}}). \quad (11)$$

The cross-entropy loss is given by,

$$\mathcal{L}_{\text{label}} = - \frac{1}{N} \sum_{i=1}^N \log \hat{\mathbf{y}}_i^{\text{GBK}} \mathbf{y}_{0,i}^{\text{train}}, \quad (12)$$

where $\hat{\mathbf{y}}_i^{\text{GBK}}$ represents the i -th row vectors of $\hat{\mathbf{Y}}^{\text{GBK}}$. Finally, we can have the integrated loss of RED

$$\mathcal{L}_{\text{RED}} = \lambda \mathcal{L}_{\text{feature}} + (1 - \lambda) \mathcal{L}_{\text{label}}, \quad (13)$$

where λ is the parameter for balancing the contribution of the teacher model and the labels.

Thus, we can merge the knowledge from two sources with extra knowledge of labels injected. Following the RED, the trained CNN backbone is frozen and serves as the backbone.

Why RED Needs Two Sources of Supervision? RED is designed to improve the representation of the backbone trained in the base phase by integrating supervised information with general knowledge. Depending exclusively on labels can result in direct adaptation to base phase labels, potentially causing forgetting in subsequent learning phases. Relying solely on the feature distribution from the SFD backbone may not be entirely effective because it could potentially mislead the GBK backbone. Hence, a fusion of both knowledge sources is crucial, a pattern supported by our experimental findings (refer to Section 4.5).

Enhancing Future Representations with a Frozen Backbone. Existing ACL methods are constrained by limited representations. Backbones trained through SL struggle to effectively capture the distinctive features of forthcoming categories, thereby restricting the performance of linear classifiers. The general knowledge learned without the labels is highly transferable in the future phases and our proposed representation enhancement incorporates general knowledge and information under supervision. Although the backbone is frozen after RED,

it yields more distinguishable representations, thereby facilitating classification in CIL. Although training the backbone during CIL can directly improve future representations, it can easily result in catastrophic forgetting on the old phases and yields a bad performance. Freezing the backbone presents an effective strategy to mitigate forgetting, inspiring the development of various CIL techniques based on a frozen backbone [38, 54] including ACL methods. REAL aligns with these CIL techniques, offering improved representations for future tasks.

3.3. Analytic Classifier with Feature Fusion

Upon obtaining the enhanced backbone via RED, we employ AL to achieve weight-invariance in classifier during the incremental learning process. Following RED, the backbone is frozen, and the classifier is replaced with an analytic classifier comprising a buffer layer and a FCN. The buffer layer, a common component in existing ACL techniques, introduces a non-linear mapping that projects features into a higher-dimensional space [7]. According to Cover's theorem, non-linear mapping to higher-dimensional space enhances feature separability [55]. However, existing ACL techniques utilize the buffer solely to process the final output of the backbone, potentially neglecting the transferable knowledge embedded in the backbone. We address this limitation by introducing the Feature Fusion Buffer (FFB) to enhance the exploitation of knowledge acquired in the base phase.

Feature Fusion Buffer. Feature maps attained by different blocks of a CNN can indicate different semantic information, where the shallow features are more transferable and the deep features can be more specific [13]. We propose a feature fusion process to utilize all these features. At phase 0, suppose the output feature map of i -th block of the CNN backbone is denoted as $\mathbf{X}_0^i \in \mathbb{R}^{N_k \times c_i \times w_i \times h_i}$, then the output after the FFB $\mathbf{X}_0^{(\text{FFB})}$ can be obtained using the following equations

$$\mathbf{X}_0^{(\text{FFB})} = \frac{1}{N_b} \sum_{i=1}^{N_b} \sigma(f_{\text{ap}}(\mathbf{X}_0^i \mathbf{W}_{i,B})), \quad (14)$$

where f_{ap} denotes the operation of the average pooling on the dimension of w_i and h_i , $\mathbf{W}_{i,B} \in \mathbb{R}^{c_i \times d_B}$ represents a randomly initialized matrix for projecting to d_B dimensional space, N_b indicates the total number of layers in CNN, and σ represents a non-linear activation function (we use ReLU in this paper). This average pooling summarizes the channel-wise information within each block, providing diversified information for the classifier training.

The benefit of FFB can be summarized in three folds: (1) FFB adheres to the benefit of projecting features into a high-dimensional space, enhancing the separability of features based on Cover's theorem. (2) FFB provides more informative features that contain transferable knowledge, thus benefits the incremental learning. (3) FFB is training-free, making it an easy yet effective technique to enhance the classifier training in ACL.

The FFB shares similar idea of utilizing multi-layer features in F-OAL [40], however, FFB further proposes a channel-wise

information condensation of each layer. Based on Vision Transformer [56], the feature fusion in F-OAL simply takes the average of class token in each layer. FFB in REAL, by contrast, utilizes an extra pooling to compress and summarize channel-wise information to provide more diversified features. The feature maps of each channel provide different perspectives of the input image [57] and previous study demonstrates the effectiveness of channel-wise information [19], making FFB an effective module in the continual learning of CNNs.

Classifier Training via Analytic Learning. Following the feature fusion, the features are provided to the subsequent FCN layer and the AL is used to train the FCN. Following the ACL process [7], the weight of the FCN layer can be obtained at the base phase by optimizing the following equation

$$\underset{\mathbf{W}_A}{\text{argmin}} \quad \|\mathbf{Y}_0^{\text{train}} - \mathbf{X}_0^{(\text{FFB})} \mathbf{W}_A^{(0)}\|_F^2 + \gamma \|\mathbf{W}_A^{(0)}\|_F^2, \quad (15)$$

where $\|\cdot\|_F^2$ is Frobenius-norm, γ is the regularization factor, $\mathbf{W}_A^{(0)}$ denotes the weight of FCN layer at the base phase, and $\mathbf{Y}_0^{\text{train}}$ denotes the stacked one-hot label tensor.

The optimal solution to (15) is

$$\hat{\mathbf{W}}_A^{(0)} = (\mathbf{X}_0^{(\text{FFB})T} \mathbf{X}_0^{(\text{FFB})} + \gamma \mathbf{I})^{-1} \mathbf{X}_0^{(\text{FFB})T} \mathbf{Y}_0^{\text{train}}, \quad (16)$$

where $\hat{\mathbf{W}}_A^{(0)}$ indicates the estimated weight of the FCN layer at phase 0, and \cdot^T represents the matrix transpose operator.

For the learning in subsequent phases, let

$$\mathbf{X}_{0:k}^{(\text{FFB})} = \begin{bmatrix} \mathbf{X}_0^{(\text{FFB})} \\ \mathbf{X}_1^{(\text{FFB})} \\ \vdots \\ \mathbf{X}_k^{(\text{FFB})} \end{bmatrix}, \quad \mathbf{Y}_{0:k}^{\text{train}} = \begin{bmatrix} \mathbf{Y}_0^{\text{train}} \\ \mathbf{Y}_1^{\text{train}} \\ \vdots \\ \mathbf{Y}_k^{\text{train}} \end{bmatrix} \quad (17)$$

At phase k , the learning problem of all seen data $\mathcal{D}_{0:k}^{\text{train}}$ can be extended from (15) to

$$\underset{\mathbf{W}_A^{(k)}}{\text{argmin}} \quad \|\mathbf{Y}_{0:k}^{\text{train}} - \mathbf{X}_{0:k}^{(\text{FFB})} \mathbf{W}_A^{(k)}\|_F^2 + \gamma \|\mathbf{W}_A^{(k)}\|_F^2. \quad (18)$$

The solution of (18) is

$$\hat{\mathbf{W}}_A^{(k)} = (\mathbf{X}_{0:k}^{(\text{FFB})T} \mathbf{X}_{0:k}^{(\text{FFB})} + \gamma \mathbf{I})^{-1} \mathbf{X}_{0:k}^{(\text{FFB})T} \mathbf{Y}_{0:k}^{\text{train}}. \quad (19)$$

The goal for CIL is to sequentially learn new tasks on $\mathcal{D}_k^{\text{train}}$ given a network trained on $\mathcal{D}_{0:k-1}^{\text{train}}$. Here, to cancel reliance on previous data in (18), let $\mathbf{R}_k = (\mathbf{X}_{0:k}^{(\text{FFB})T} \mathbf{X}_{0:k}^{(\text{FFB})} + \gamma \mathbf{I})$ and $\mathbf{Q}_k = \mathbf{X}_{0:k}^{(\text{FFB})T} \mathbf{Y}_{0:k}^{\text{train}}$, the problem can be solved in the following transformation,

$$\begin{aligned} \hat{\mathbf{W}}_A^{(k)} &= \mathbf{R}_k^{-1} \mathbf{Q}_k \\ &= \left(\sum_{i=0}^k \mathbf{X}_i^{(\text{FFB})T} \mathbf{X}_i^{(\text{FFB})} + \gamma \mathbf{I} \right)^{-1} \sum_{i=0}^k \mathbf{X}_i^{(\text{FFB})T} \mathbf{Y}_i^{\text{train}} \\ &= (\mathbf{R}_{k-1} + \mathbf{X}_k^{(\text{FFB})T} \mathbf{X}_k^{(\text{FFB})})^{-1} (\mathbf{Q}_{k-1} + \mathbf{X}_k^{(\text{FFB})T} \mathbf{Y}_k^{\text{train}}), \end{aligned} \quad (20)$$

where $\mathbf{X}_i^{(\text{FFB})}$ denotes the feature tensor after FFB at phase i .

Equation (20) indicates that the results of joint training in (18) can be reproduced by sequentially performing recursively training on $\mathcal{D}_k^{\text{train}}$. That is, the information of previous phases 0:k-1 can be encoded in \mathbf{R}_{k-1} and \mathbf{Q}_{k-1} , and the new information can be included via addition, as expressed in Equation (20). This implies the property that CIL is equalized to joint training with both present and historical data, i.e., the *weight-invariant property* [7] shared in the ACL family. This pattern ensures the non-forgetting in ACL and yields high performance. Our proposed REAL model also adheres to this property, exhibiting strong performance in mitigating forgetting. Additionally, by leveraging RED and FFB, the proposed REAL model can further enhance the efficacy of training features within the FCN, significantly improving performance compared to ACL techniques.

Incorporate REAL into DS-AL. Here, we demonstrate how REAL can be effectively integrated into another ACL technique, namely DS-AL [12], which enhances ACIL by introducing a compensation stream to learn residues. Following DS-AL, we incorporate a compensation stream into REAL and refer to this modified version as REAL-DS. REAL-DS maintains the same paradigm of backbone training to utilize RED and the modification lies on the ALFF.

At phase k, upon learning from the labels (i.e., the main stream), the training of the compensation stream to fit the residuals commences. Let $\tilde{\mathbf{Y}}_k$ denote the residue of final output after conducting the main stream, which is calculated as

$$\tilde{\mathbf{Y}}_k = \mathbf{Y}_k^{\text{train}} - \mathbf{X}_k^{(\text{FFB})} \hat{\mathbf{W}}_A^{(k)}[:, : -d_{yk}], \quad (21)$$

where $\mathbf{X}_k^{(\text{FFB})} \hat{\mathbf{W}}_A^{(k)}[:, : -d_{yk}]$ represents the logits of current learning classes and d_{yk} indicates the number of the classes in phase k. Equation (21) computes the local residue for the current learning phase, and a compensation stream is employed to rectify this error. The objective of the compensation stream is to

$$\underset{\mathbf{W}_{A,C}^{(k)}}{\text{argmin}} \quad \left\| \tilde{\mathbf{Y}}_k - \mathbf{X}_{0:k,C}^{(\text{FFB})} \mathbf{W}_{A,C}^{(k)} \right\|_F^2 + \gamma \left\| \mathbf{W}_{A,C}^{(k)} \right\|_F^2, \quad (22)$$

where $\mathbf{X}_{C,0:k}^{(\text{FFB})} = \frac{1}{N_b} \sum_{i=1}^{N_b} \sigma_C(f_{\text{ap}}(\mathbf{X}_{0:k}^i) \mathbf{W}_{i,B})$ represents the input of the compensation stream with activation function σ_C , which is used to alternate the input of the compensation stream to improve the fitting ability [12]. The solution to Equation (22) is

$$\hat{\mathbf{W}}_{A,C}^{(k)} = (\mathbf{R}_{k-1,C} + \mathbf{X}_{k,C}^{(\text{FFB})\text{T}} \mathbf{X}_{k,C}^{(\text{FFB})})^{-1} (\mathbf{Q}_{k-1,C} + \mathbf{X}_{k,C}^{(\text{FFB})\text{T}} \tilde{\mathbf{Y}}_k), \quad (23)$$

$$\mathbf{R}_{k-1,C} = (\mathbf{X}_{0:k-1,C}^{(\text{FFB})\text{T}} \mathbf{X}_{0:k-1,C}^{(\text{FFB})} + \gamma \mathbf{I}), \quad \mathbf{Q}_{k-1,C} = \mathbf{X}_{0:k-1,C}^{(\text{FFB})\text{T}} \tilde{\mathbf{Y}}_{0:k-1}, \quad (24)$$

which completes the learning of the compensation stream. The inference with compensation stream is produced by combining both streams as $\hat{\mathbf{Y}}_k = \mathbf{X}_k^{(\text{FFB})} \hat{\mathbf{W}}_A^{(k)} + C \mathbf{X}_{k,C}^{(\text{FFB})} \hat{\mathbf{W}}_{A,C}^{(k)}$, where C is the factor to control the contribution of compensation stream.

Accordingly, our REAL can be an seamlessly integrate into DS-AL. This demonstrates that, REAL can function as a plug-and-play module capable of improving established ACL techniques via enhanced representations and informative features.

4. Experiments

This section discusses comprehensive experiments on various benchmark datasets to validate REAL. First, we compare the proposed REAL with various EFCIL and EBCIL methods. Subsequently, the analysis on hyperparameters, representation enhancement and ablation study of knowledge sources in REAL are provided.

4.1. Experimental Setup

Datasets. We evaluate the performance of REAL together with existing ACL methods on CIFAR-100 [58], ImageNet-100 [19], and ImageNet-1k [59]. CIFAR-100 contains 100 classes of 32×32 color images with each class containing 500 images for training and 100 images for testing respectively. ImageNet-1k has 1.3 million images for training and 50,000 images for testing within 1000 classes. ImageNet-100, as defined in [19], is constructed by selecting 100 specific classes from ImageNet-1k.

CIL Protocol. For CIL evaluation, we follow the protocol adopted in various CIL studies [19, 60, 36], which involves partitioning the dataset into a base training set (i.e., phase 0) and a sequence of incremental sets. The base dataset contains half of the full data classes. The network is first trained on the base dataset. Subsequently, the network gradually learns the remaining classes evenly for K phases. In the experiment, we report the results for phase $K = 5, 10, 25$, and 50 on CIFAR-100 and ImageNet-100. Additionally, we validate our REAL on ImageNet-1k with $K = 5, 10$, and 25.

Implementation Details. The architecture in the experiment is ResNet-18 [61]. Additionally, we train a ResNet-32 on CIFAR-100 as many CIL methods (e.g., [7] and [23]) adopt this structure. All the experiments of CIL are conducted on an NVIDIA GeForce RTX 3090 GPU with Python 3.9, PyTorch 1.13.1, and TorchVision 0.14.1 with PyCIL [62].

During the DS-BPT, we adopt the following parameter settings. For the GBK acquisition stream, we adopt the same training strategies for SSCL in [49] and train the backbones for 1000, 600, and 100 epochs on CIFAR-100, ImageNet-100, and Imagenet-1k respectively, using SGD with a momentum of 0.9 and an initial learning rate of 0.1. The learning rates decay in a cosine manner, and the value for weight decay is 5×10^{-4} . The batch size for training is 512. The projector and predictor comprise 2-layer MLPs with batch normalization incorporated after the FCNs. During training, under the setting of stopping gradients in Simsim [49], only the gradients of features produced by the network containing the predictor are backpropagated. For data augmentation in the GBK acquisition, we use the combination of *RandomResizedCrop*, *RandomHorizontalFlip*, and *ColorJitter*. For the SFD learning stream, we follow DS-AL [12] to train the networks using SGD for 160 (90) epochs for ResNet-32 on CIFAR-100 (ResNet-18). The learning rate starts at 0.1 and is divided by 10 at epoch 80 (30) and 120 (60). We adopt a momentum of 0.9 and weight decay of 5×10^{-4} (1×10^{-4}) with a batch size of 128. No special data augmentation exists in SFD learning.

Table 1: Comparison of average accuracy $\bar{\mathcal{A}}$ and last-phase accuracy \mathcal{A}_K among EFCIL and replay-based methods on CIFAR-100. We use both backbones of ResNet-32 and ResNet-18 for fair comparison. Data in Bold indicate the best within EFCIL methods and data underlined are the best considering both EFCIL and EBCIL. "EF" is the abbreviation of exemplar-free. "K" indicates the number of phases.

Backbone	Method	EF?	$\bar{\mathcal{A}}(\%)$				$\mathcal{A}_K(\%)$			
			K=5	10	25	50	K=5	10	25	50
ResNet-32	LUCIR [18]	×	63.17	60.14	57.54	55.57	54.30	50.30	48.35	42.10
	PODNet [19]	×	64.83	63.19	60.72	59.10	54.60	53.00	51.40	46.64
	POD+AAANets [24]	×	66.31	64.31	62.31	59.15	59.39	57.37	53.55	49.40
	POD+AAANets+RMM [23]	×	68.36	66.67	64.12	63.54	59.00	59.03	56.50	54.3
	FOSTER [20]	×	<u>72.58</u>	67.95	65.67	59.57	<u>65.57</u>	58.44	56.15	52.23
	LwF [4]	✓	49.59	48.47	45.75	10.19	40.40	40.19	38.25	2.09
	ACIL [7]	✓	66.30	66.07	65.95	66.01	57.78	57.79	57.65	57.83
	DS-AL [12]	✓	66.46	66.22	66.13	66.33	58.14	58.12	58.19	58.37
	REAL (ours)	✓	68.78	68.62	68.60	68.41	61.19	61.15	61.46	61.32
REAL-DS (ours)	✓	68.88	68.75	68.79	68.42	61.62	61.76	62.18	61.87	
ResNet-18	PASS [36]	✓	63.88	60.07	56.86	41.11	55.75	49.13	44.76	28.02
	PRAKA [14]	✓	68.59	68.51	62.98	43.09	61.52	60.12	51.15	27.14
	ACIL [7]	✓	68.07	68.08	68.07	67.94	60.65	61.03	61.41	61.09
	DS-AL [12]	✓	68.55	68.23	68.20	68.17	61.35	61.31	61.41	61.41
	REAL (ours)	✓	72.35	72.41	72.28	72.25	65.73	65.86	65.81	65.76
	REAL-DS (ours)	✓	72.24	72.35	72.20	72.23	66.27	66.74	66.57	66.35

For RED, we adopt the learning epochs $e = \{50, 50, 100\}$ and balancing factor $\lambda = \{0.5, 0.5, 0.9\}$ on CIFAR-100, ImageNet-100, and ImageNet-1k. For AL in REAL and REAL-DS, we follow ACIL and DS-AL to adopt $\gamma = 1e - 5$ and $d_B = 15k$. In REAL-DS, following [12], the compensation ratio is adopted as $C = \{0.6, 0.8, 1.4\}$ on CIFAR100, ImageNet-100, and ImageNet-1k respectively.

Evaluation Protocol. We adopt two metrics for evaluation, *average incremental accuracy* and *last-phase accuracy*. The overall performance is evaluated by the *average incremental accuracy* (or *average accuracy*) $\bar{\mathcal{A}} = \frac{1}{K+1} \sum_{k=0}^K \mathcal{A}_k$, where \mathcal{A}_k indicates the average test accuracy at phase k obtained by testing on $\mathcal{D}_{0:k}^{\text{test}}$. A higher $\bar{\mathcal{A}}$ score is preferred at evaluations. The other metric *last-phase accuracy* \mathcal{A}_K measures the last-phase performance of the network after completing all CIL tasks. \mathcal{A}_K is an important metric as it reveals the gap between CIL joint training, a gap all CIL methods aim to close.

4.2. Comparison with State-of-the-Art Methods

To validate the performance of our methods, we compare them with both exemplar-based and exemplar-free methods. Results on CIFAR-100, ImageNet-100, and ImageNet-1k are presented in Table 1, 2, and 3 respectively.

Baselines. For exemplar-free methods, we validate REAL with LwF [4], PASS [36], PRAKA [14], ACIL [7] and DS-AL [12]. Among these techniques, LwF is a regularization-based method that uses KD to construct a regularization term in objective function, PASS and PRAKA are within the category of prototype-based methods, and ACIL and DS-AL are ACL techniques. Additionally, we include exemplar-based methods, i.e., LUCIR [18], PODNet [19], AAANets [24], RMM [23] and FOSTER [20], as counterpart. For the compared methods, we follow the official implementations from their papers.

Validation on CIFAR-100. As depicted in Table 1, on CIFAR-100, we validate REAL with ResNet-18 and ResNet-32 as several compared methods are implemented with different backbones. The results for CIFAR-100 in Table 1 underscore the competitive performance of EBCIL methods, owing to the benefits of sample storage and exemplar replay. Notably, with a smaller K (e.g., $K = 5, 10$), FOSTER achieves the best results among all compared methods. However, the ACL techniques (ACIL and DS-AL) marginally lag behind "POD+AAANets+RMM" in these settings. Through representation enhancement, our REAL elevates ACL methods to approach or even surpass the performance of state-of-the-art EBCIL methods with a small K of 5. For instance, REAL-DS demonstrates superior results in both average accuracy and final phase accuracy when compared with "POD+AAANets+RMM". With a larger K of 10 or more, REAL-DS even outperforms the leading exemplar-based method, FOSTER, and maintains this trend with increasing K . Among the EFCIL methods, the compared ACL methods (i.e., ACIL and DS-AL) have already shown competitive performance on various settings of K with both ResNet-18 and ResNet-32. As a new technique within the ACL family, our REAL can have improved performance and achieve best performance among the EFCIL methods. For example, the average accuracy results of REAL-DS with $K = 5, 10, 25$, and 50 with ResNet-18, are 72.24%, 72.35%, 72.20%, and 72.23% respectively, surpassing the previous ACL baseline DS-AL with 3.69%, 4.12%, 4.00%, and 4.06% respectively. Notably, as K increases, all EBCIL and EFCIL methods except ACL experience a notable performance decline. For instance, the final phase accuracy results of FOSTER and PRAKA drop from 68.57% and 61.52% to 52.23% each when K rises from 5 to 50. By contrast, the ACL techniques, including REAL and REAL-DS, maintain consistent performance irrespective of the

Table 2: Comparison of average accuracy $\bar{\mathcal{A}}$ and last-phase accuracy \mathcal{A}_K on ImageNet-100. Data in Bold indicate the best within EFCIL methods and data underlined are the best considering both EFCIL and EBCIL. "EF" is the abbreviation of exemplar-free. "K" indicates the number of phases.

Backbone	Method	EF?	$\bar{\mathcal{A}}(\%)$				$\mathcal{A}_K(\%)$			
			K=5	10	25	50	K=5	10	25	50
ResNet-18	LUCIR [18]	×	71.32	68.57	61.57	51.08	60.00	57.10	49.26	43.13
	PODNet [19]	×	75.90	73.70	66.58	59.36	67.60	65.00	54.30	44.40
	POD+AAANets [24]	×	76.96	75.58	71.78	64.63	69.40	67.47	63.69	51.00
	POD+AAANets+RMM [23]	×	79.52	<u>78.47</u>	76.54	71.21	73.80	<u>71.40</u>	68.84	56.50
	FOSTER [20]	×	<u>79.94</u>	<u>77.73</u>	71.79	66.77	<u>74.52</u>	<u>70.54</u>	62.70	59.20
	LwF [4]	✓	54.12	47.90	44.45	13.13	<u>40.10</u>	36.10	34.12	2.30
	PASS [36]	✓	72.24	67.97	52.02	30.59	61.76	57.38	37.46	18.22
	PRAKA [14]	✓	63.66	62.75	58.86	41.24	55.77	54.77	46.49	21.80
	ACIL [7]	✓	74.81	74.76	74.59	74.57	66.98	67.42	67.16	67.38
	DS-AL [12]	✓	75.08	75.89	74.70	74.78	67.54	67.38	67.32	67.50
	REAL (ours)	✓	76.48	76.39	76.14	76.20	68.94	69.18	69.00	69.02
	REAL-DS (ours)	✓	77.30	77.32	<u>77.19</u>	<u>77.11</u>	69.52	69.82	69.76	69.46

Table 3: Comparison of average accuracy $\bar{\mathcal{A}}$ and last-phase accuracy \mathcal{A}_K on ImageNet-1k. Data in Bold indicate the best within EFCIL methods and data underlined are the best considering both EFCIL and EBCIL. EF is the abbreviation of exemplar-free. "K" indicates the number of phases.

Backbone	Method	EF?	$\bar{\mathcal{A}}(\%)$			$\mathcal{A}_K(\%)$		
			K=5	10	25	K=5	10	25
ResNet-18	LUCIR [18]	×	64.45	61.57	56.56	56.60	51.70	46.23
	PODNet [19]	×	66.43	63.20	59.17	58.90	55.70	50.51
	POD+AAANets [24]	×	67.73	64.85	61.78	60.84	57.22	53.21
	POD+AAANets+RMM [23]	×	<u>69.21</u>	67.45	63.93	<u>62.50</u>	<u>60.10</u>	55.50
	FOSTER [20]	×	61.65	60.74	57.64	<u>51.45</u>	49.60	46.80
	LwF [4]	✓	44.35	38.90	36.87	34.20	30.10	30.01
	PASS [36]	✓	58.44	56.44	52.41	49.83	47.71	42.55
	PRAKA [14]	✓	51.71	49.48	45.56	44.35	41.85	36.54
	ACIL [7]	✓	65.34	64.84	61.78	56.11	55.43	55.43
	DS-AL [12]	✓	67.15	66.98	66.88	58.12	58.20	58.12
	REAL (ours)	✓	67.41	67.18	67.15	58.06	58.06	58.14
	REAL-DS (ours)	✓	68.04	<u>67.78</u>	<u>67.60</u>	59.39	59.35	<u>59.33</u>

number of learning phases. This observation showcases that REAL maintains the invariance of phases inherent in ACL and take advantage of this property in large learning phases.

Validation on ImageNet-100 and ImageNet-1k. As indicated in Table 2, the leading patterns of REAL and REAL-DS persist when compared with EFCIL methods. Notably, REAL outperforms the current state-of-the-art EFCIL method DS-AL by significant margins in both average incremental accuracy and final phase accuracy. The advantage of maintaining weight invariance across phases enables REAL and REAL-DS to deliver exceptional performance even with larger K values. When compared with EBCIL methods, the trend of leading in scenarios with large K is consistent with that observed on CIFAR-100. EBCIL methods excel in leveraging exemplar replay in settings with small K , while REAL leads when K reaches 10 or higher. On ImageNet-1k, REAL and REAL-DS continue to outperform other EFCIL methods, and the leading pattern compared to EBCIL methods aligns with observations on ImageNet-100.

Evolution Curves of Phase-wise Accuracy. We present the

evolution curves of phase-wise accuracy on all datasets in Figure 3 to comprehensively visualize the results. We plot the results phase-wise accuracy of LUCIR, PODNet, POD+AAANets, POD+AAANets+RMM, FOSTER, PASS, PRAKA, ACIL, DS-AL and our proposed REAL-DS. The EBCIL methods are plotted in dash lines. As illustrated in Figure 3, REAL-DS achieves the highest performance among all benchmark datasets when compared with EFCIL methods. The leading trend commences from the base phase and is consistently maintained through to the final phase, underscoring exceptional performance of REAL-DS during the incremental learning process. When contrasted with EBCIL methods, REAL-DS exhibits a more gradual decline trend when a larger $K = 25, 50$ is employed. This trend indicates that REAL-DS effectively addresses larger learning phases and surpass the compared methods.

4.3. Forgetting Analysis

We propose a comparative study on the average forgetting rate $\bar{\mathcal{F}}$ [40] between REAL and the existing methods to analyze

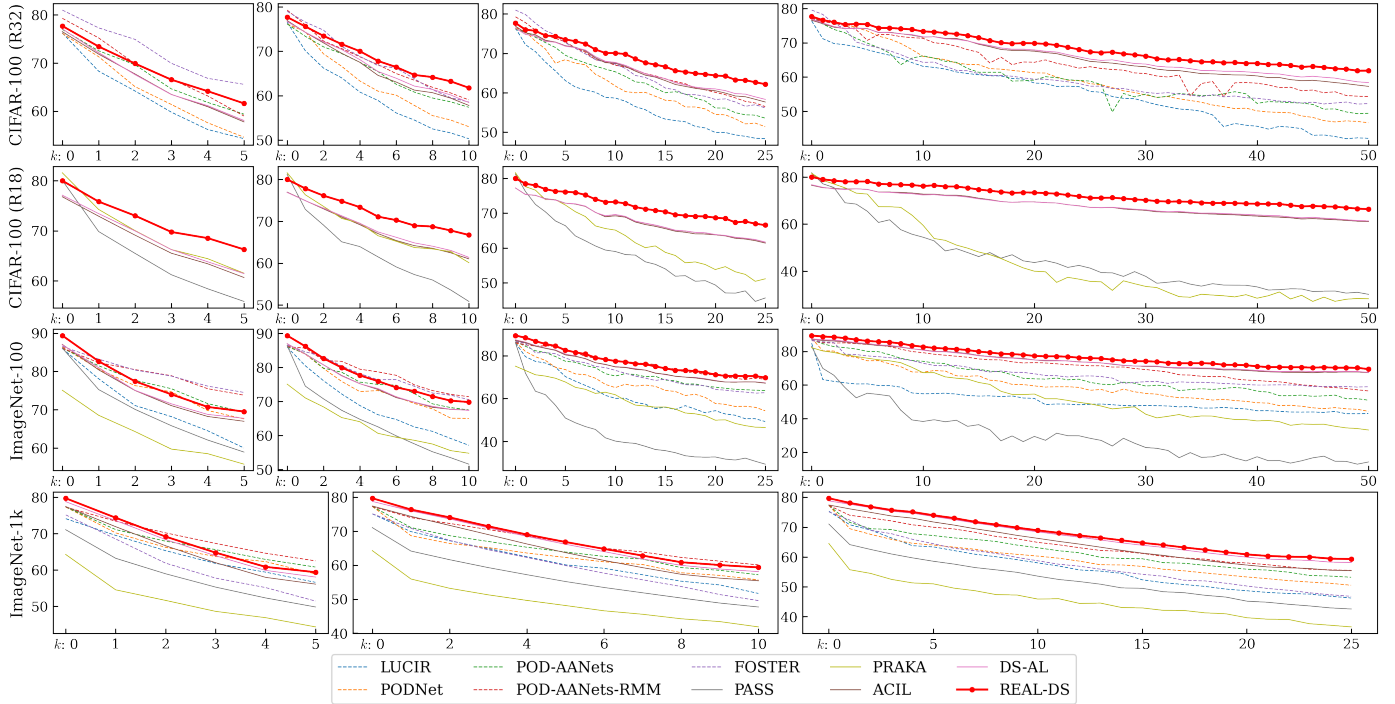


Figure 3: Phase-wise accuracy of compared methods on benchmark datasets with $K = 5, 10, 25,$ and 50 on CIFAR-100 and ImageNet-100. The results of ImageNet-1k with $K = 5, 10, 25$ are also included. The dash lines are the curves for exemplar-based methods. ‘‘CIFAR-100 (R32)’’ denotes the results on CIFAR-100 with backbone of ResNet-32, while ‘‘R18’’ indicates using the ResNet-18. Experiments without specific denotation use ResNet-18 as the backbone.

REAL’s performance of reducing forgetting. A lower average forgetting rate shows a better performance of resisting forgetting during the incremental learning process. The average forgetting rate is defined as $\bar{\mathcal{F}} = \frac{1}{K} \sum_{k=1}^K \mathcal{F}_k$, where \mathcal{F}_k denotes the forgetting rate at phase k obtained by testing the model of phase k on previous data then comparing this accuracy with the optimal previous results. The \mathcal{F}_k can be obtained by:

$$\mathcal{F}_k = \frac{1}{k} \sum_{j=0}^{k-1} f_{k,j}, \quad f_{k,j} = \max_{l \in \{1, \dots, k-1\}} (\mathcal{A}_{l,j}) - \mathcal{A}_{k,j}, \quad \forall j < k,$$

where $\mathcal{A}_{k,j}$ denotes accuracy evaluated on the test set of phase j after training the network at phase k .

As indicated in Table 4, REAL and REAL-DS demonstrate superior performance of reducing forgetting when compared with other methods on both CIFAR-100 and ImageNet-100. For example, REAL achieves the $\bar{\mathcal{F}}$ of 4.66%, 4.05%, 3.96%, and 4.22% on CIFAR-100 with $K=5, 10, 25,$ and 50 respectively, outperforming PASS and even the exemplar-based methods (PODNet and FOSTER) with large gaps. When compared with ACL techniques, REAL and REAL-DS have lower forgetting rates, demonstrating the effect of well mitigating forgetting introduced by RED and FFD.

4.4. Ablation Study

Ablation Study on RED and FFB. In this section, we explore the efficacy of each component in the proposed REAL model, specifically the RED and FFB modules. We perform the experiments on CIFAR-100 and ImageNet-100 using ResNet-18 in the 5-phase CIL setting and present the results in Table

Table 4: Comparison of average forgetting $\bar{\mathcal{F}}$ (%) on CIFAR-100 and ImageNet-1k. Data in Bold indicate the best results within compared methods. ‘‘K’’ indicates the number of phases.

Method	CIFAR-100				ImageNet-100			
	K=5	10	25	50	K=5	10	25	50
PODNet [19]	15.64	20.71	24.93	30.07	14.91	18.26	24.35	26.29
FOSTER [20]	13.12	18.28	21.58	27.45	12.14	15.21	25.22	35.39
PASS [36]	16.09	20.05	23.18	30.71	10.44	18.43	28.32	35.92
ACIL [7]	5.46	4.61	4.85	5.41	6.54	7.09	9.09	9.52
DS-AL [12]	6.41	5.98	5.80	6.08	8.07	9.79	11.34	11.69
REAL (ours)	4.66	4.05	3.96	4.22	5.68	7.79	7.13	8.49
REAL-DS (ours)	5.81	4.77	4.55	4.88	6.16	8.20	8.71	10.31

5. To validate the effectiveness of RED, we utilize the backbones with GBK and SFD as two distinct knowledge sources and merge two streams with RED. As indicated in the Table 5, without FFB, the backbone with SFD outperforms that with GBK on CIFAR-100 in terms of both \mathcal{A}_K and $\bar{\mathcal{A}}$. Contrastingly, the results are reversed on ImageNet-100, highlighting the advantages of general knowledge on larger datasets. This observation indicates that general knowledge can be more effectively on a larger dataset owing to the abundance of training samples, while a smaller dataset relies more on labels to guide the learning process. By utilizing RED to merge these two types of knowledge, the model achieves significantly better performance than models trained on single knowledge sources. This underscores that the knowledge fusion enabled by RED leverages the strengths of both knowledge types, enhancing the performance of base model in incremental learning. Since SFD is obtained by the cross entropy loss and the GBK is obtained

by training with SSCL loss, this study demonstrates the benefit of leveraging both types of training techniques. Furthermore, upon incorporating FFB, performance with all backbones is improved, indicating that FFB can effectively generate informative features.

Table 5: Ablation study of the knowledge components in REAL.

Knowledge Sources	FFB	CIFAR-100		ImageNet-100	
		\mathcal{A}_K (%)	$\bar{\mathcal{A}}$ (%)	\mathcal{A}_K (%)	$\bar{\mathcal{A}}$ (%)
GBK	×	57.01	62.66	67.42	74.48
	✓	60.22	64.88	67.98	74.76
SFD	×	60.91	68.21	65.64	73.56
	✓	62.41	69.23	67.28	74.36
Merging with RED	×	64.98	71.85	68.36	76.01
	✓	65.72	72.34	68.94	76.48

RED Surpasses Directly Using Two Base Training Losses.

In the base training, REAL captures the general knowledge and class-specific knowledge via SSCL and SL respectively (DS-BPT), and then merges them via RED. A simpler approach is to directly utilize the SSCL and SL loss jointly to formulate a joint training loss during base training. Here, we use the same parameters and conduct a comparative study on RED and the training with joint training loss on CIFAR-100. The joint loss can be formulated as $\mathcal{L}_{\text{joint}} = \alpha \mathcal{L}_{\text{label}} + \beta \mathcal{L}_{\text{GBK}}$, where α and β are the balancing coefficients. As indicated in Table 6, REAL outperforms the results of various combinations of α and β . This observation showcases the superiority of RED in merging the general knowledge and class-specific knowledge. The reason that joint training loss falls behind may be that, these two goals may have conflicts and this training can lose the soft knowledge of SFD. Since the SSCL considers the sample-wise similarities while the SL loss primarily focuses on the category-wise discrepancy, they may affect each other and satisfying these two objectives together in the early stages may be hard to achieve. Also, RED leverages the soft knowledge of SFD, leading to a superior performance when compared with directly using the joint objective.

Table 6: Comparative study of RED and directly using two base training losses of SSCL and SL.

Base Training Loss	\mathcal{A}_K (%)	$\bar{\mathcal{A}}$ (%)
$\alpha = 1.0, \beta = 0.1$	53.40	64.01
$\alpha = 1.0, \beta = 0.5$	54.89	65.35
$\alpha = 1.0, \beta = 1.0$	56.95	66.93
$\alpha = 0.5, \beta = 1.0$	56.51	66.74
$\alpha = 0.1, \beta = 1.0$	49.27	56.74
REAL (ours)	65.73	72.35

Comparative Study between REAL and SupCon. Supervised contrastive loss (SupCon) [63] represents a loss of contrastive learning with the label information. Here, we propose a comparative study between REAL and SupCon on CIFAR-100 for $K = 5$. The results of various settings of epoch (e) and batch size (bsz) are tabulated in Table 7. SupCon achieves similar results to the GBK only (e.g., 56.80% and 64.31% of SupCon($e = 200, bsz = 2048$) vs 57.01% and 62.66% of \mathcal{A}_K and $\bar{\mathcal{A}}$ respectively) but falls behind REAL, which demonstrates that, though SupCon is a contrastive learning method

based on the label information, it may not benefit as effective as the CE loss. REAL outperforms the results obtained by different parameter settings and demonstrates its effectiveness of merging general knowledge stems from the contrastive learning and the class-specific knowledge from SL.

Table 7: Comparative study of REAL and using SupCon loss in the base training. “e” denotes the epochs and “bsz” denotes the batch size.

Base Training Loss	\mathcal{A}_K (%)	$\bar{\mathcal{A}}$ (%)
SupCon($e = 200, bsz = 512$)	54.52	63.33
SupCon($e = 200, bsz = 1024$)	54.68	63.65
SupCon($e = 200, bsz = 2048$)	56.80	64.31
SupCon($e = 500, bsz = 512$)	56.49	65.96
SupCon($e = 500, bsz = 1024$)	55.31	64.55
SupCon($e = 500, bsz = 2048$)	54.77	63.94
GBK only	57.01	62.66
REAL (ours)	65.73	72.35

REAL Improves Both Stability and Plasticity. Here, we investigate the impact of each component of REAL on the stability and plasticity by ablating RED and FFB. To demonstrate this, after training on all phases, we evaluate the models on the base dataset $\mathcal{D}_0^{\text{test}}$ (i.e., the first half) to show the stability and the CIL dataset $\mathcal{D}_{1:K}^{\text{test}}$ (i.e., the other half) to evaluate the plasticity. The experiments are conducted on CIFAR-100 and ImageNet-100. We report the accuracy on base dataset $\mathcal{A}_{K,0}$, the accuracy on CIL dataset $\mathcal{A}_{K,1:K}$, and last phase accuracy \mathcal{A}_K in Figure 4. Without any modification, the baseline of only SFD obtains relatively low performance on both $\mathcal{A}_{K,0}$ and $\mathcal{A}_{K,1:K}$ and then results in a low performance of \mathcal{A}_K . When RED is included, the results of both $\mathcal{A}_{K,0}$ and $\mathcal{A}_{K,1:K}$ improve significantly, demonstrating RED can enhance both stability and plasticity. The enhanced plasticity can be attributed to the discriminative capabilities provided by GBK acquisition. In particular, GBK aids in distinguishing data categories not encountered by the backbone during the base phase, thereby facilitating classification during incremental learning. On the stability front, REAL enriches data representations during the base phase, thereby reinforcing foundational knowledge. With the inclusion of FFB, the performance can be further improved in terms of both stability and plasticity. FFB fuses both the transferable and specific features, ultimately improving the overall stability and plasticity of the model.

Visualization of Representation Enhancement. To demonstrate the effect of RED and FFB, we conduct a qualitative study by visualizing feature vectors in 2D with t-SNE [64]. The feature vectors are extracted on the validation set of ImageNet-100 by randomly choosing 5 classes from the base dataset and 2 classes from CIL dataset. As depicted in Figure 5, with REAL, the feature vectors within a category exhibit a clustering effect, where vectors belonging to the same category are pulled closer together compared to the baseline model without RED and FFB. This clustering phenomenon is evident within base classes (e.g., classes 3 and 12) and extends to classes that are not directly learned in the base phase (i.e., classes 85 and 99). By bringing features within the same category closer together, REAL facilitates the construction of more discriminative decision boundaries, thereby enhancing the overall performance.

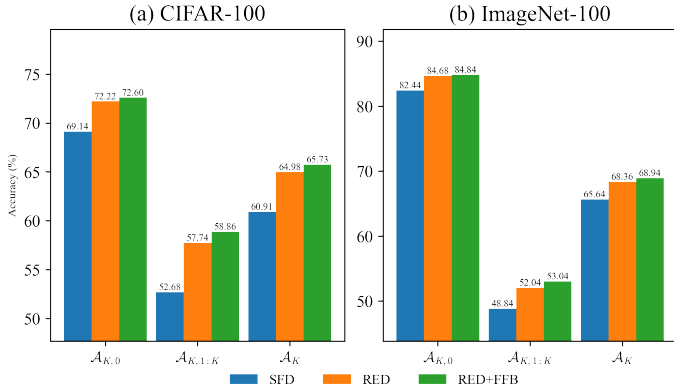


Figure 4: Analysis on stability and plasticity by ablating RED and FFB.

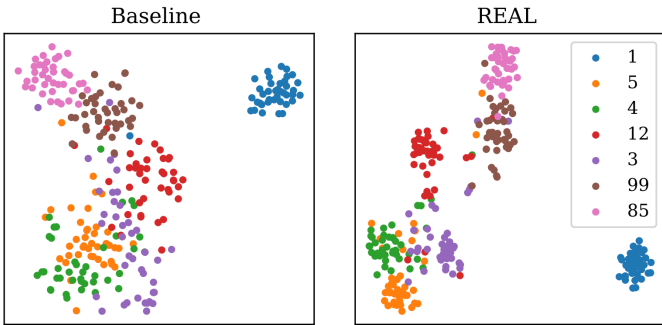


Figure 5: T-SNE plot of feature vectors extracted on ImageNet-100. The features extracted with REAL within a class are more compact compared with those in the baseline.

Plug and Play Technique for ACL Branch. To validate the compatibility of REAL with more ACL methods, we conduct further experiments of incorporating REAL into another ACL method GKEAL [11] on CIFAR-100 and ImageNet-100. As indicated in Table 8, when incorporating REAL into GKEAL, the results on both the CIFAR-100 and ImageNet-100 are improved across all K values. For example, on CIFAR-100, REAL can improve the \mathcal{A}_K GKEAL from 57.65% to 61.54%. This observation further demonstrates that REAL can be a beneficial plug-and-play technique for ACL methods.

Table 8: Comparison of the average accuracy and $\bar{\mathcal{A}}(\%)$ and the last-phase accuracy \mathcal{A}_K between GKEAL and introducing REAL to GKEAL (denoted as REAL-GKEAL) on CIFAR-100 and ImageNet-1k. “ K ” indicates the number of phases.

Dataset	Method	\mathcal{A}_K			$\bar{\mathcal{A}}$		
		K=5	10	25	K=5	10	25
CIFAR-100	GKEAL	57.65	57.65	57.65	66.72	66.54	66.43
	REAL-GKEAL	61.54	61.54	61.54	70.82	70.60	70.41
ImageNet-100	GKEAL	64.52	64.52	64.52	73.06	72.85	72.77
	REAL-GKEAL	64.96	64.96	64.96	74.87	74.62	74.50

4.5. Hyperparameter Analysis

Balancing Labels and Teacher Model with λ . To analyze the impact of λ , we conduct the experiments with a 5-phase CIL setting and the results of \mathcal{A}_K and $\bar{\mathcal{A}}$ from $\lambda = 0.0$ to $\lambda = 1.0$ are plotted in Figure 6. Across all three benchmark datasets,

the performance initially improves with larger λ values, reaching a peak before decreasing. This trend highlights the balance between knowledge derived from the labels and the feature distribution learned by the backbone. The optimal λ values that result in the best performance increase as the dataset scales up, transitioning from $\lambda = 0.5$ on CIFAR-100 and ImageNet-100 to $\lambda = 0.9$ on ImageNet-1k. This pattern shows that models trained on larger datasets tend to prefer knowledge from the feature distribution learned in the backbone. Feature distributions acquired from extensive datasets, for example, the ImageNet-1k, are potent and highly transferable owing to the abundance of training samples available. During the RED process, the SFD knowledge is transferred to the backbone with GBK and contributes more than the labels solely. Notably, utilizing only labels ($\lambda = 0.0$) or solely relying on the backbone with SFD ($\lambda = 1.0$) results in less effective performance across all three datasets. This observation underscores the benefits of combining feature distribution with labels in enhancing model performance.

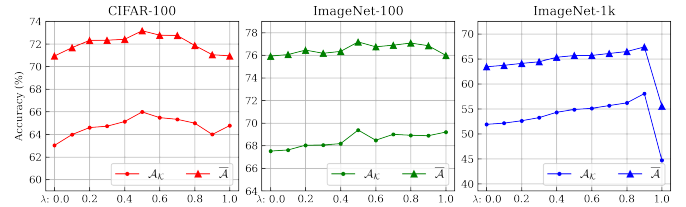


Figure 6: Accuracy on benchmark datasets with varying λ .

Study on the Buffer Size of FFB. To analyze the impact of buffer size d_B on the FF module, we conduct the experiments with $d_B = \{1k, 2k, 3k, 5k, 8k, 10k, 12k, 15k, 18k, 20k\}$ on CIFAR-100 under the 5-phase setting. We further extend the experiments of $d_B = \{23k, 25k, 28k, 29k\}$ on ImageNet-100 (a d_B larger than 29k will run out of memory). The results of average accuracy and last phase accuracy are depicted in Figure 7. On CIFAR-100, the performance of REAL first increases as d_B scales up. The performance reaches the peak at $d_B = 12k$. On ImageNet-100, a similar trend is observed as d_B increases from $d_B = 1k$ to $d_B = 29k$ and the performance reaches the peak at $d_B = 15k$. This pattern shows that, the projection to relatively high dimensional space can boost the effect of the FFB module and choices of $d_B = 15k$ for both datasets yields good performance for REAL.

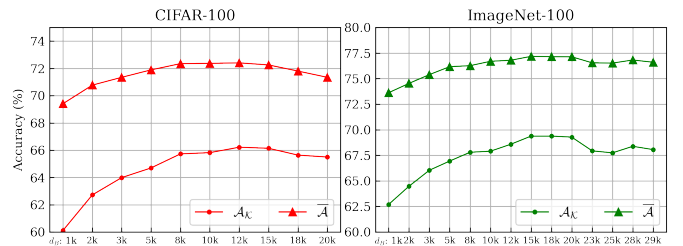


Figure 7: Accuracy on CIFAR-100 and ImageNet-100 with varying d_B .

5. Conclusions

In this paper, we propose Representation Enhanced Analytic Learning (REAL) for EFCIL. To address the limitation of representation, REAL leverages a dual-stream base pretraining (DS-BPT) to initialize the network with base knowledge. DS-BPT combines a stream for general base knowledge acquisition via self-supervised contrastive learning (SSCL) and a stream for learning supervised feature distribution via supervised learning. The subsequent process of representation enhancing distillation (RED) in REAL enriches the SSCL pre-trained backbones with additional knowledge obtained under supervision. This process enhances the ability of the backbone to extract effective features at both base phase and unseen categories in future phases, greatly facilitating subsequent stages of analytic class-incremental learning. REAL addresses the underutilization of backbone knowledge by introducing the feature fusion buffer (FFB) to provide informative features. FFB merges information from various backbone layers to create features with both transferable and specific information, thereby enhancing subsequent classifier training. Moreover, REAL can be seamlessly integrated into existing ACL techniques, including DS-AL. Comprehensive experiments and analysis validate the effectiveness of REAL. Empirical results showcase that REAL surpasses existing EFCIL methods and even outperforms most EBCIL methods.

CRedit Authorship Contribution Statement

Run He: Conceptualization, Investigation, Methodology, Implementation, Data Curation, Writing – original draft. Di Fang: Methodology, Implementation, Writing – review & editing. Yizhu Chen: Methodology, Implementation, Writing – review & editing. Kai Tong: Methodology, Writing – review & editing. Cen Chen: Writing – review & editing. Yi Wang: Writing – review & editing. Lap-Pui Chau: Writing – review & editing. Huiping Zhuang: Conceptualization, Supervision, Writing – review & editing.

Declaration of Competing Interest

The authors declare that they have no known competing financial interests or personal relationships that could have appeared to influence the work reported in this paper.

Data Availability

All datasets used in the paper are publicly available.

Funding

This work was supported in part by National Natural Science Foundation of China (Grant No. 62306117), in part by Guangzhou Basic and Applied Basic Research Foundation (Grant No. 2024A04J3681), and in part by GJYC Program of Guangzhou (Grant No. 2024D03J0005).

References

[1] Z. Fu, Z. Wang, X. Xu, M. Yang, Z. Chi, W. Ding, Semantic alignment with self-supervision for class incremental

learning, *Knowledge-Based Systems* 282 (2023) 111114. doi:10.1016/j.knosys.2023.111114.

[2] R. Chen, X.-Y. Jing, F. Wu, H. Chen, Sharpness-aware gradient guidance for few-shot class-incremental learning, *Knowledge-Based Systems* 299 (2024) 112030. doi:10.1016/j.knosys.2024.112030.

[3] H. yang Lu, L. kang Lin, C. Fan, C. Wang, W. Fang, X. jun Wu, Knowledge-guided prompt-based continual learning: Aligning task-prompts through contrastive hard negatives, *Knowledge-Based Systems* 310 (2025) 113009. doi:10.1016/j.knosys.2025.113009.

[4] Z. Li, D. Hoiem, Learning without forgetting, *IEEE Transactions on Pattern Analysis and Machine Intelligence* 40 (12) (2018) 2935–2947.

[5] S.-A. Rebuffi, A. Kolesnikov, G. Sperl, C. H. Lampert, iCaRL: Incremental classifier and representation learning, in: *Proceedings of the IEEE Conference on Computer Vision and Pattern Recognition (CVPR)*, 2017.

[6] E. Belouadah, A. Popescu, I. Kanellos, A comprehensive study of class incremental learning algorithms for visual tasks, *Neural Networks* 135 (2021) 38–54.

[7] H. Zhuang, Z. Weng, H. Wei, R. XIE, K.-A. Toh, Z. Lin, ACIL: Analytic class-incremental learning with absolute memorization and privacy protection, in: S. Koyejo, S. Mohamed, A. Agarwal, D. Belgrave, K. Cho, A. Oh (Eds.), *Advances in Neural Information Processing Systems*, Vol. 35, Curran Associates, Inc., 2022, pp. 11602–11614.

[8] P. Guo, M. R. Lyu, N. Mastorakis, Pseudoinverse learning algorithm for feedforward neural networks, *Advances in Neural Networks and Applications* (2001) 321–326.

[9] H. Zhuang, Z. Lin, K.-A. Toh, Blockwise recursive Moore-Penrose inverse for network learning, *IEEE Transactions on Systems, Man, and Cybernetics: Systems* (2021) 1–14.

[10] H. Zhuang, Z. Lin, K.-A. Toh, Correlation projection for analytic learning of a classification network, *Neural Processing Letters* (2021) 1–22.

[11] H. Zhuang, Z. Weng, R. He, Z. Lin, Z. Zeng, GKEAL: Gaussian kernel embedded analytic learning for few-shot class incremental task, in: *Proceedings of the IEEE/CVF Conference on Computer Vision and Pattern Recognition (CVPR)*, 2023, pp. 7746–7755.

[12] H. Zhuang, R. He, K. Tong, Z. Zeng, C. Chen, Z. Lin, DS-AL: A dual-stream analytic learning for exemplar-free class-incremental learning, *Proceedings of the AAAI Conference on Artificial Intelligence* 38 (15) (2024) 17237–17244. doi:10.1609/aaai.v38i15.29670.

- [13] J. Yosinski, J. Clune, Y. Bengio, H. Lipson, How transferable are features in deep neural networks?, in: Z. Ghahramani, M. Welling, C. Cortes, N. Lawrence, K. Weinberger (Eds.), *Advances in Neural Information Processing Systems*, Vol. 27, Curran Associates, Inc., 2014.
- [14] W. Shi, M. Ye, Prototype reminiscence and augmented asymmetric knowledge aggregation for non-exemplar class-incremental learning, in: *Proceedings of the IEEE/CVF International Conference on Computer Vision (ICCV)*, 2023, pp. 1772–1781.
- [15] L. Jing, Y. Tian, Self-supervised visual feature learning with deep neural networks: A survey, *IEEE Transactions on Pattern Analysis and Machine Intelligence* 43 (11) (2021) 4037–4058. doi:10.1109/TPAMI.2020.2992393.
- [16] X. Tao, X. Chang, X. Hong, X. Wei, Y. Gong, Topology-preserving class-incremental learning, in: A. Vedaldi, H. Bischof, T. Brox, J.-M. Frahm (Eds.), *Computer Vision – ECCV 2020*, Springer International Publishing, Cham, 2020, pp. 254–270.
- [17] C. Simon, P. Koniusz, M. Harandi, On learning the geodesic path for incremental learning, in: *Proceedings of the IEEE/CVF Conference on Computer Vision and Pattern Recognition (CVPR)*, 2021, pp. 1591–1600.
- [18] S. Hou, X. Pan, C. C. Loy, Z. Wang, D. Lin, Learning a unified classifier incrementally via rebalancing, in: *Proceedings of the IEEE/CVF Conference on Computer Vision and Pattern Recognition (CVPR)*, 2019.
- [19] A. Douillard, M. Cord, C. Ollion, T. Robert, E. Valle, PodNet: Pooled outputs distillation for small-tasks incremental learning, in: *Computer Vision–ECCV 2020: 16th European Conference, Glasgow, UK, August 23–28, 2020, Proceedings, Part XX 16*, Springer, 2020, pp. 86–102.
- [20] F.-Y. Wang, D.-W. Zhou, H.-J. Ye, D.-C. Zhan, FOSTER: Feature boosting and compression for class-incremental learning, in: S. Avidan, G. Brostow, M. Cissé, G. M. Farinella, T. Hassner (Eds.), *Computer Vision – ECCV 2022*, Springer Nature Switzerland, Cham, 2022, pp. 398–414.
- [21] R. Aljundi, E. Belilovsky, T. Tuytelaars, L. Charlin, M. Caccia, M. Lin, L. Page-Caccia, Online continual learning with maximal interfered retrieval, in: H. Wallach, H. Larochelle, A. Beygelzimer, F. d'Alché-Buc, E. Fox, R. Garnett (Eds.), *Advances in Neural Information Processing Systems*, Vol. 32, Curran Associates, Inc., 2019.
- [22] A. Prabhu, P. H. S. Torr, P. K. Dokania, GDumb: A simple approach that questions our progress in continual learning, in: A. Vedaldi, H. Bischof, T. Brox, J.-M. Frahm (Eds.), *Computer Vision – ECCV 2020*, Springer International Publishing, Cham, 2020, pp. 524–540.
- [23] Y. Liu, B. Schiele, Q. Sun, RMM: Reinforced memory management for class-incremental learning, *Advances in Neural Information Processing Systems* 34 (2021).
- [24] Y. Liu, B. Schiele, Q. Sun, Adaptive aggregation networks for class-incremental learning, in: *Proceedings of the IEEE/CVF Conference on Computer Vision and Pattern Recognition (CVPR)*, 2021, pp. 2544–2553.
- [25] Y. Liu, Y. Li, B. Schiele, Q. Sun, Online hyperparameter optimization for class-incremental learning, *Proceedings of the AAAI Conference on Artificial Intelligence* 37 (7) (2023) 8906–8913. doi:10.1609/aaai.v37i7.26070.
- [26] R. Aljundi, F. Babiloni, M. Elhoseiny, M. Rohrbach, T. Tuytelaars, Memory aware synapses: Learning what (not) to forget, in: V. Ferrari, M. Hebert, C. Sminchisescu, Y. Weiss (Eds.), *Computer Vision – ECCV 2018*, Springer International Publishing, Cham, 2018, pp. 144–161.
- [27] D. Li, Z. Zeng, CRNet: A fast continual learning framework with random theory, *IEEE Transactions on Pattern Analysis and Machine Intelligence* 45 (9) (2023) 10731–10744. doi:10.1109/TPAMI.2023.3262853.
- [28] J. Schwarz, W. Czarnecki, J. Luketina, A. Grabska-Barwinska, Y. W. Teh, R. Pascanu, R. Hadsell, Progress and Compress: A scalable framework for continual learning, in: J. Dy, A. Krause (Eds.), *Proceedings of the 35th International Conference on Machine Learning*, Vol. 80 of *Proceedings of Machine Learning Research*, PMLR, 2018, pp. 4528–4537.
- [29] L. Yu, B. Twardowski, X. Liu, L. Herranz, K. Wang, Y. Cheng, S. Jui, J. v. d. Weijer, Semantic drift compensation for class-incremental learning, in: *Proceedings of the IEEE/CVF Conference on Computer Vision and Pattern Recognition (CVPR)*, 2020.
- [30] M. Toldo, M. Ozay, Bring evanescent representations to life in lifelong class incremental learning, in: *Proceedings of the IEEE/CVF Conference on Computer Vision and Pattern Recognition (CVPR)*, 2022, pp. 16732–16741.
- [31] S. Wang, W. Shi, Y. He, Y. Yu, Y. Gong, Non-exemplar class-incremental learning via adaptive old class reconstruction, in: *Proceedings of the 31st ACM International Conference on Multimedia, MM '23*, Association for Computing Machinery, New York, NY, USA, 2023, p. 4524–4534. doi:10.1145/3581783.3611926.
- [32] P. Dhar, R. V. Singh, K.-C. Peng, Z. Wu, R. Chellappa, Learning without memorizing, in: *Proceedings of the IEEE/CVF Conference on Computer Vision and Pattern Recognition (CVPR)*, 2019.
- [33] J. Kirkpatrick, R. Pascanu, N. Rabinowitz, J. Veness, G. Desjardins, A. A. Rusu, K. Milan, J. Quan, T. Rammalho, A. Grabska-Barwinska, et al., Overcoming catastrophic forgetting in neural networks, *Proceedings of the national academy of sciences* 114 (13) (2017) 3521–3526.

- [34] F. Zenke, B. Poole, S. Ganguli, Continual learning through synaptic intelligence, in: D. Precup, Y. W. Teh (Eds.), Proceedings of the 34th International Conference on Machine Learning, Vol. 70 of Proceedings of Machine Learning Research, PMLR, 2017, pp. 3987–3995.
- [35] A. Chaudhry, P. K. Dokania, T. Ajanthan, P. H. S. Torr, Riemannian walk for incremental learning: Understanding forgetting and intransigence, in: V. Ferrari, M. Hebert, C. Sminchisescu, Y. Weiss (Eds.), Computer Vision – ECCV 2018, Springer International Publishing, Cham, 2018, pp. 556–572.
- [36] F. Zhu, X.-Y. Zhang, C. Wang, F. Yin, C.-L. Liu, Prototype augmentation and self-supervision for incremental learning, in: Proceedings of the IEEE/CVF Conference on Computer Vision and Pattern Recognition (CVPR), 2021, pp. 5871–5880.
- [37] K. Zhu, W. Zhai, Y. Cao, J. Luo, Z.-J. Zha, Self-sustaining representation expansion for non-exemplar class-incremental learning, in: Proceedings of the IEEE/CVF Conference on Computer Vision and Pattern Recognition (CVPR), 2022, pp. 9296–9305.
- [38] G. Petit, A. Popescu, H. Schindler, D. Picard, B. Delezoide, FeTrIL: Feature translation for exemplar-free class-incremental learning, in: Proceedings of the IEEE/CVF Winter Conference on Applications of Computer Vision (WACV), 2023, pp. 3911–3920.
- [39] T. Malepathirana, D. Senanayake, S. Halgamuge, NAPA-VQ: Neighborhood-aware prototype augmentation with vector quantization for continual learning, in: Proceedings of the IEEE/CVF International Conference on Computer Vision (ICCV), 2023, pp. 11674–11684.
- [40] H. Zhuang, Y. Liu, R. He, K. Tong, Z. Zeng, C. Chen, Y. Wang, L.-P. Chau, F-OAL: Forward-only online analytic learning with fast training and low memory footprint in class incremental learning, in: A. Globerson, L. Mackey, D. Belgrave, A. Fan, U. Paquet, J. Tomczak, C. Zhang (Eds.), Advances in Neural Information Processing Systems, Vol. 37, Curran Associates, Inc., 2024, pp. 41517–41538.
- [41] D. Fang, Y. Zhu, Z. Lin, C. Chen, Z. Zeng, H. Zhuang, AIR: Analytic imbalance rectifier for continual learning (2024). [arXiv:2408.10349](https://arxiv.org/abs/2408.10349).
- [42] H. Zhuang, D. Fang, K. Tong, Y. Liu, Z. Zeng, X. Zhou, C. Chen, Online analytic exemplar-free continual learning with large models for imbalanced autonomous driving task, IEEE Transactions on Vehicular Technology 74 (2) (2025) 1949–1958. doi:10.1109/TVT.2024.3483557.
- [43] H. Zhuang, Y. Chen, D. Fang, R. He, K. Tong, H. Wei, Z. Zeng, C. Chen, GAEL: Exemplar-free generalized analytic continual learning, in: A. Globerson, L. Mackey, D. Belgrave, A. Fan, U. Paquet, J. Tomczak, C. Zhang (Eds.), Advances in Neural Information Processing Systems, Vol. 37, Curran Associates, Inc., 2024, pp. 83024–83047.
- [44] X. Yue, X. Zhang, Y. Chen, C. Zhang, M. Lao, H. Zhuang, X. Qian, H. Li, MMAL: Multi-modal analytic learning for exemplar-free audio-visual class incremental tasks, in: Proceedings of the 32nd ACM International Conference on Multimedia, MM ’24, Association for Computing Machinery, New York, NY, USA, 2024, pp. 2428–2437. doi:10.1145/3664647.3681607.
- [45] Y. Xu, Y. Chen, J. Nie, Y. Wang, H. Zhuang, M. Okumura, Advancing cross-domain discriminability in continual learning of vision-language models, in: The Thirty-eighth Annual Conference on Neural Information Processing Systems, 2024.
- [46] T. Chen, S. Kornblith, M. Norouzi, G. Hinton, A simple framework for contrastive learning of visual representations, in: H. D. III, A. Singh (Eds.), Proceedings of the 37th International Conference on Machine Learning, Vol. 119 of Proceedings of Machine Learning Research, PMLR, 2020, pp. 1597–1607.
- [47] K. He, H. Fan, Y. Wu, S. Xie, R. Girshick, Momentum contrast for unsupervised visual representation learning, in: Proceedings of the IEEE/CVF Conference on Computer Vision and Pattern Recognition (CVPR), 2020.
- [48] J.-B. Grill, F. Strub, F. Altché, C. Tallec, P. Richemond, E. Buchatskaya, C. Doersch, B. Avila Pires, Z. Guo, M. Gheshlaghi Azar, B. Piot, k. kavukcuoglu, R. Munos, M. Valko, Bootstrap your own latent - a new approach to self-supervised learning, in: H. Larochelle, M. Ranzato, R. Hadsell, M. Balcan, H. Lin (Eds.), Advances in Neural Information Processing Systems, Vol. 33, Curran Associates, Inc., 2020, pp. 21271–21284.
- [49] X. Chen, K. He, Exploring simple siamese representation learning, in: Proceedings of the IEEE/CVF Conference on Computer Vision and Pattern Recognition (CVPR), 2021, pp. 15750–15758.
- [50] X. Liu, F. Zhang, Z. Hou, L. Mian, Z. Wang, J. Zhang, J. Tang, Self-supervised learning: Generative or contrastive, IEEE Transactions on Knowledge and Data Engineering 35 (1) (2023) 857–876. doi:10.1109/TKDE.2021.3090866.
- [51] H. Cha, J. Lee, J. Shin, Co2L: Contrastive continual learning, in: Proceedings of the IEEE/CVF International Conference on Computer Vision (ICCV), 2021, pp. 9516–9525.
- [52] E. Fini, V. G. T. da Costa, X. Alameda-Pineda, E. Ricci, K. Alahari, J. Mairal, Self-supervised models are continual learners, in: Proceedings of the IEEE/CVF Conference on Computer Vision and Pattern Recognition (CVPR), 2022, pp. 9621–9630.

- [53] G. Petit, M. Soumm, E. Feillet, A. Popescu, B. Delezoide, D. Picard, C. Hudelot, An analysis of initial training strategies for exemplar-free class-incremental learning, in: *Proceedings of the IEEE/CVF Winter Conference on Applications of Computer Vision (WACV)*, 2024, pp. 1837–1847.
- [54] D. Goswami, Y. Liu, B. o. Twardowski, J. van de Weijer, FeCAM: Exploiting the heterogeneity of class distributions in exemplar-free continual learning, in: *Advances in Neural Information Processing Systems*, Vol. 36, Curran Associates, Inc., 2023, pp. 6582–6595.
- [55] T. M. Cover, Geometrical and statistical properties of systems of linear inequalities with applications in pattern recognition, *IEEE Transactions on Electronic Computers* EC-14 (3) (1965) 326–334. doi:10.1109/PGEC.1965.264137.
- [56] A. Dosovitskiy, L. Beyer, A. Kolesnikov, D. Weissenborn, X. Zhai, T. Unterthiner, M. Dehghani, M. Minderer, G. Heigold, S. Gelly, J. Uszkoreit, N. Houlsby, An image is worth 16x16 words: Transformers for image recognition at scale, in: *International Conference on Learning Representations*, 2021.
URL <https://openreview.net/forum?id=YicbFdNTTy>
- [57] Y. Zou, S. Zhang, H. Zhou, Y. Li, R. Li, Compositional few-shot class-incremental learning, in: R. Salakhutdinov, Z. Kolter, K. Heller, A. Weller, N. Oliver, J. Scarlett, F. Berkenkamp (Eds.), *Proceedings of the 41st International Conference on Machine Learning*, Vol. 235 of *Proceedings of Machine Learning Research*, PMLR, 2024, pp. 62964–62977.
URL <https://proceedings.mlr.press/v235/zou24c.html>
- [58] A. Krizhevsky, G. Hinton, et al., Learning multiple layers of features from tiny images (2009).
- [59] O. Russakovsky, J. Deng, H. Su, J. Krause, S. Satheesh, S. Ma, Z. Huang, A. Karpathy, A. Khosla, M. Bernstein, et al., ImageNet large scale visual recognition challenge, *International Journal of Computer Vision* 115 (3) (2015) 211–252.
- [60] Y. Liu, Y. Su, A.-A. Liu, B. Schiele, Q. Sun, Mnemonics training: Multi-class incremental learning without forgetting, in: *Proceedings of the IEEE/CVF Conference on Computer Vision and Pattern Recognition (CVPR)*, 2020.
- [61] K. He, X. Zhang, S. Ren, J. Sun, Deep residual learning for image recognition, in: *Proceedings of the IEEE Conference on Computer Vision and Pattern Recognition (CVPR)*, 2016.
- [62] D.-W. Zhou, F.-Y. Wang, H.-J. Ye, D.-C. Zhan, PyCIL: a python toolbox for class-incremental learning, *Science China Information Sciences* 66 (9) (2023) 197101. doi:10.1007/s11432-022-3600-y.
- [63] P. Khosla, P. Teterwak, C. Wang, A. Sarna, Y. Tian, P. Isola, A. Maschinot, C. Liu, D. Krishnan, Supervised contrastive learning, in: H. Larochelle, M. Ranzato, R. Hadsell, M. Balcan, H. Lin (Eds.), *Advances in Neural Information Processing Systems*, Vol. 33, Curran Associates, Inc., 2020, pp. 18661–18673.
URL https://proceedings.neurips.cc/paper_files/paper/2020/file/d89a66c7c80a29b1bdbab0f2a1a94af8-Paper.pdf
- [64] L. Van der Maaten, G. Hinton, Visualizing data using t-SNE, *Journal of machine learning research* 9 (11) (2008).